CFD Modeling of Large-Scale Pool Fires

Arnaud Trouvé

**Department of Fire Protection Engineering, University of Maryland,
College Park, MD, U.S.A.**
atrouve@umd.edu

Abstract

We review in this study current numerical and modeling challenges found in a computational fluid dynamics (CFD) treatment of large-scale pool fires. The numerical challenge comes from the need to suitably resolve flame geometries that are significantly more complex than those found at laboratory scales. The flame geometries found in large-scale pool fires correspond to multiple, relatively small flames and the increased small-scale activity results in more severe computational grid requirements. The modeling challenge comes from the need to provide adequate descriptions of flame extinction and soot processes. Flame extinction, soot mass leakage across the flame and the subsequent accumulation of cold soot in the overfire region are identified as key physical ingredients that will determine the performance of fire models in large-scale pool fire simulations. Current CFD capabilities are illustrated using the Fire Dynamics Simulator (FDS, developed by the National Institute of Standards and Technology, USA). FDS is applied to a series of numerical simulations corresponding to open, wind-free, gaseous pool fires of different sizes H, $0.4 \leq H \leq 40$ m. The simulations reveal the fundamental change in flame structure that is observed as H is increased from laboratory- to large-scales. Predictions of combustion efficiencies, soot yields and radiant fractions show limited success, however. Some modifications in the FDS combustion and soot models are proposed in order to enhance the modeling capability. These modifications are based on the assumptions that: (1) flame extinction in pool fires correspond to slow mixing conditions combined with radiation cooling; (2) flame extinction is the dominant mechanism responsible for soot mass leakage across the flame. FDS simulations performed with these modifications show improved performance and provide some encouraging support to the assumptions made.

1. Introduction

Liquid or gaseous fuel pool fires correspond to one of the generic configurations considered in fire science. Open or confined pool fire configurations are often used for basic studies of the structure and dynamics of fires, *e.g.*, basic studies of the buoyancy-driven turbulent flow coupled with fuel-air mixing and non-premixed combustion, soot formation processes, and smoke and thermal radiation emissions. In the case of liquid fuels, pool fire configurations also provide a simple flame/fuel-source geometry to study the gas-to-liquid thermal feedback that drives the fuel mass loss rate and determines the overall fire size. Finally, pool fire configurations are representative of real-world fire hazards, for instance spilling/leaking fuel tank fires as found in home, tank farm or transportation accident scenarios.

Previous studies have shown that the pool size (*i.e.*, the effective fuel source diameter D) has an important impact on the fire structure and dynamics [1-8]. Different flow, heat transfer and combustion regimes are observed as D is increased from laboratory-scales ($D \leq 1$-3 m) to field-scales ($D \geq 1$-3 m). A first transition is observed as the flow evolves from laminar to turbulent: small-diameter pools ($D \leq 0.1$ m) feature (steady or unsteady) laminar flow, whereas large-diameter pools ($D \geq 1$ m) are fully turbulent, and intermediate values ($0.1 \leq D \leq 1$ m) correspond to a transitional regime. A second transition is observed in the case of liquid fuels as the gas-to-liquid thermal feedback evolves from a convective- to a radiation-dominated regime: convective heat transfer dominates the heat feedback in small-diameter pools ($D \leq 0.1$ m), whereas radiative heat transfer dominates at large diameters ($D \geq 0.5$-1 m); and intermediate values ($0.1 \leq D \leq 0.5$-1 m) correspond to a mixed regime. Finally, a third transition is observed in the case of hydrocarbon sooty fuels as the combustion evolves from quasi-complete to strongly-incomplete conditions: in small-diameter pools ($D \leq 0.1$ m), soot is confined to the underfire region, whereas at large diameters ($D \geq 1$ m), soot is also present in the overfire region, *i.e.*, the fire experiences a transition from "sooting" to "smoking" conditions. Beyond this third transition, much of the fire becomes surrounded by layers of cold soot (*i.e.*, black smoke) that dramatically increase the optical thickness as well as decrease the radiant emission of the fire. In this large-scale regime ($D \geq 2$-3 m), pool fires of increasing diameter exhibit decreasing values of the combustion efficiency χ_a (defined as the ratio of the heat release rate $\dot{Q}$

divided by the product of the fuel mass loss rate $\dot{m}_F$ times the ideal heat of combustion ΔH_F^{th}, $\chi_a = \dot{Q}/(\dot{m}_F \Delta H_F^{th})$), increasing values of the smoke yield η_{soot} (defined as the ratio of the soot mass emission rate divided by the fuel mass loss rate, $\eta_{soot} = (\dot{m}_{soot}/\dot{m}_F)$), and decreasing values of the radiant fraction χ_R (defined as the overall radiative cooling rate $\dot{Q}_R$ divided by the product of the fuel mass loss rate times the ideal heat of combustion, $\chi_R = \dot{Q}_R/(\dot{m}_F \Delta H_F^{th})$).

Combustion efficiency, smoke yield and radiant fraction are closely related quantities in pool fires: increased levels of smoke emission in the overfire region [9-11] are generally associated with more frequent flame extinction phenomena (*i.e.*, lower combustion efficiencies) [3]; cold soot in the overfire region is in turn responsible for the blockage effect that explains the drop in radiant fraction [5]. Experimental data on combustion efficiencies or smoke yields in intermediate- or large-scale pool fires are scarce in the technical literature. Data on combustion efficiencies in gaseous fuel pool fires are presented as a function of the fuel mass loss rate (per unit fuel source area) $\dot{m}_F''$ in [12], for different fuels (methane, propane and acetylene) and different burner diameters (up to $D = 1$ m); it is found that in the case of acetylene, the combustion efficiency decreases when the fuel mass loss rate is increased, and takes values as low as 80% for $\dot{m}_F'' = 0.02\ \text{kg/m}^2/\text{s}$. Data on smoke yields in liquid fuel pool fires are presented as a function of the pool diameter in [9-11]; it is found that smoke yields increase with D, and take values as high as 15% for $D \geq 2\text{-}3$ m. Experimental data on radiant fractions in pool fires, ranging from small- to large-scales, are more common. For instance, Koseki and co-workers report measurements of the radiant fraction in pool fires over a wide range of diameters and for different engineering liquid fuels (heptane, gasoline, kerosene, crude oil and JP-4) [4,13-14]: it is found that while for $D \leq 2\text{-}3$ m, the radiant fraction takes large constant values, $\chi_R \approx 0.4$, χ_R drops rapidly at larger diameters ($\chi_R < 0.05$ for $D \approx 50$ m). Yang, Hamins and Kashiwagi [15] explain these results by performing a scaling analysis that suggests that while the radiant fraction is size-independent at low values of D ($D \leq 1$ m), χ_R scales like D to the power one-half at larger diameters ($D \geq 1$ m), $\chi_R \sim D^{-1/2}$.

In addition to changes in χ_a, χ_R and η_{soot}, previous studies also reveal a dramatic change in flame shape and height as the pool diameter is increased to very large values [16-21]. This change is generally discussed in terms of the non-dimensional fire size $\dot{Q}^* = \dot{Q}/(\rho_\infty c_{p,\infty} T_\infty g^{1/2} D^{5/2})$, where ρ_∞, $c_{p,\infty}$ and T_∞ are the mass density, specific heat (at constant pressure) and temperature of ambient air, and g the magnitude of the gravity acceleration. At moderate-to-small values of $\dot{Q}^*$ ($\dot{Q}^* \geq 1$, *i.e.*, at small-to-moderate values of D), the fire features a classical cone-shaped single-flame geometry, while the flame height L_f scales almost linearly with D, and is several times larger than D, $L_f > D$; in contrast, at very-small-values of $\dot{Q}^*$ ($\dot{Q}^* \leq 0.2$, *i.e.*, at very-large values of D), the fire features multiple individual flames, while the height of those flames becomes approximately independent of D, and takes values smaller than D, $L_f \leq D$; intermediate values of $\dot{Q}^*$ ($0.2 \leq \dot{Q}^* \leq 1$) correspond to a transitional regime [17-18,20-21].
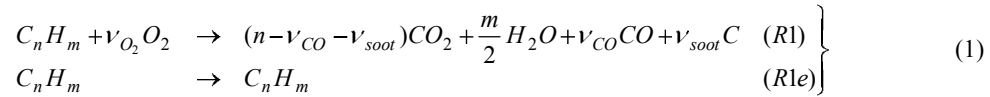
These known changes in the structure of pool fires in response to changes in size are clearly a concern since they reveal the limitations of laboratory-scale experimental studies that often correspond to transitional, weakly-turbulent flow, small-to-intermediate optical thicknesses, and single-flame, quasi-complete, weakly-smoking, turbulent combustion conditions. These conditions are not representative of the dynamics of large-scale pool fires. While CFD modeling is an attractive alternative to the experimental approach since at first sight, it is not limited to small- or intermediate-scale conditions, previous work on numerical simulations of large-scale pool fires remains limited (see [22-23] for recent examples) and the numerical and modeling challenges associated with such simulations are not fully understood.

The numerical challenge in a CFD treatment of large-scale pool fires comes from the need to provide adequate resolution of flame-based phenomena. As the pool diameter is increased, the relative flame height (L_f/D) decreases from typical values equal to 3-4 to values below 1. This corresponds to a much increased small-scale activity and higher computational grid requirements. Additional difficulties come from the need to provide adequate descriptions of flame extinction and soot formation/oxidation. The ability to meet this modeling challenge will determine in turn the ability of a fire model to simulate the dominant features of large-scale pool fires, *i.e.*, the decrease in combustion efficiency, the soot mass leakage to the overfire region and the corresponding increase in smoke yield, and the build-up of a cold soot envelope around the fire and the corresponding decrease in radiant fraction. It is worth emphasizing that the description of flame extinction and soot processes are topics of active research in the combustion science and fire science communities and that current models have not yet reached suitable levels of maturity and accuracy.

The general objective of the present study is to evaluate the ability of current fire modeling tools to simulate large-scale pool fires. We consider in the following a simplified configuration corresponding to open, wind-free, square-shaped, gaseous (propylene) pool fires with a prescribed fuel mass loss rate. The numerical simulations are performed using a CFD solver called the Fire Dynamics Simulator (FDS). FDS is developed by the National Institute of Standards and Technology (NIST), U.S.A., and is oriented towards fire applications; it uses a Large Eddy Simulation approach for turbulence (based on the classical Smagorinsky model), a fast chemistry model for non-premixed combustion (based on the Eddy Dissipation Concept), a mixture-fraction-based model for soot formation (based on a soot yield), and a radiative-transfer-equation model for thermal radiation transport (based on a gray gas or a wide band treatment) [24-25]. We present in the following results obtained in two series of FDS simulations corresponding to pool fires of different sizes. The first series uses the NIST release of FDS Version 5, herein called FDS5; these simulations provide valuable information on the changes in the fire structure that occur at larger scales but also reveal incorrect predictions of the combustion efficiency and soot yield. The second series uses a modified version of FDS, called FDS5m, in which the flame extinction model has been enhanced to include (along air vitiation effects) fuel type, fuel vitiation, and flow time scale effects; the simulations show improved performance and suggest that slow mixing and radiation extinction may be the dominant factors responsible for increased smoke emissions from large-scale pool fires.

2. Combustion and Soot Modeling in FDS5

The modeling framework in FDS Version 5 corresponds to a one-step or two-step global combustion model, with or without flame extinction due to air vitiation [25]. We limit our discussion herein to the one-step version of the combustion model. We start from the following global combustion equation:

$$\left.\begin{array}{ll} C_nH_m + \nu_{O_2}O_2 \quad \rightarrow \quad (n - \nu_{CO} - \nu_{soot})CO_2 + \dfrac{m}{2}H_2O + \nu_{CO}CO + \nu_{soot}C & (R1) \\ C_nH_m \quad \quad \quad \rightarrow \quad C_nH_m & (R1e) \end{array}\right\} \quad (1)$$

where $\nu_{O_2} = (n + (m/4) - (\nu_{CO}/2) - \nu_{soot})$. Reaction ($R1$) corresponds to the formation of combustion products (CO_2, H_2O, and also CO and soot – treated as pure carbon) while reaction ($R1e$) refers to the possible extinction of reaction ($R1$) (*e.g.*, due to air vitiation). In FDS, fuel mass is assumed to remain unchanged during extinction events and reaction ($R1e$) takes a trivial form. This assumption is questionable and will be re-visited in the next Section. The stoichiometric coefficients in reaction ($R1$) are simply obtained from the fuel chemical composition and user-specified carbon monoxide and soot yields.

In FDS5, the mixture composition is described using two reactive scalars, called Z_1 and Z_2. These scalars are based on the following decomposition of carbon mass:

$$Z = \underbrace{Y_{C_nH_m}}_{Z_1} + \underbrace{(\frac{W_{C_nH_m}}{nW_{CO_2}})Y_{CO_2} + (\frac{W_{C_nH_m}}{nW_{CO}})Y_{CO} + (\frac{W_{C_nH_m}}{nW_{soot}})Y_{soot}}_{Z_2} \quad (2)$$

where Z is the mixture fraction, Z_1 represents the carbon mass fraction contained in the fuel, and Z_2 the carbon mass fraction contained in CO_2, CO and soot, and where Y_k and W_k are the mass fraction and molecular weight of species k. It can be shown that the entire mixture composition can be reconstructed from the knowledge of Z_1 and Z_2 via state relationships. We have in particular: $Y_{soot} = (\nu_{soot}W_{soot}/W_{C_nH_m})Z_2$.

The corresponding governing equations are:

$$\left.\begin{array}{l} \dfrac{\partial}{\partial t}(\overline{\rho}\widetilde{Z}_1) + \dfrac{\partial}{\partial x_i}(\overline{\rho}\widetilde{u}_i\widetilde{Z}_1) = \dfrac{\partial}{\partial x_i}(\overline{\rho}D_t\dfrac{\partial\widetilde{Z}_1}{\partial x_i}) - \overline{\dot{\omega}}'''_{R1} \\ \\ \dfrac{\partial}{\partial t}(\overline{\rho}\widetilde{Z}_2) + \dfrac{\partial}{\partial x_i}(\overline{\rho}\widetilde{u}_i\widetilde{Z}_2) = \dfrac{\partial}{\partial x_i}(\overline{\rho}D_t\dfrac{\partial\widetilde{Z}_2}{\partial x_i}) + \overline{\dot{\omega}}'''_{R1} \end{array}\right\} \quad (3)$$

where $\overline{\dot{\omega}}'''_{R1}$ is the mass reaction rate of the global combustion reaction ($R1$). In FDS5, combustion is treated using a closure expression known as the Eddy Dissipation Concept model [26]:

$$\overline{\dot{\omega}}'''_{R1} = [1 - FEF] \times \overline{\rho} \times \frac{\min(\widetilde{Y}_F; \widetilde{Y}_{O_2}/r_s)}{\tau} \quad ; \quad \overline{\dot{\omega}}'''_{R1e} = FEF \times \overline{\rho} \times \frac{\min(\widetilde{Y}_F; \widetilde{Y}_{O_2}/r_s)}{\tau} \quad (4)$$

where r_s is the stoichiometric oxygen-to-fuel mass ratio, τ a characteristic combustion time scale, and where *FEF* is a flame extinction factor that takes values 0 or 1, and is determined according to a diffusion

flame extinction model (see below). The time scale τ is described following a classical turbulent closure expression: $\tau = C_\tau (\Delta^2 / \nu_t)$, where Δ is the computational grid cell size, ν_t the turbulent viscosity, and C_τ a model coefficient; we use $C_\tau = 0.025$.

We now turn to the diffusion flame extinction model. The FDS5 model formulation for *FEF* uses the following ingredients [27]: a critical flame temperature T_c, below which extinction is predicted to occur; a lower oxygen index, that characterizes limiting oxygen levels for flames supplied with diluted air at ambient temperature, $T_\infty = 300$ K; and a model for the flame temperature T_{st}. The critical flame temperature model may be viewed as a simplified version of a classical description based on critical values of the scalar dissipation rate [28-29]; we use $T_c \approx 1,700$K. The lower oxygen index is also described as an empirical input quantity and is specified as $Y_{O_2,c} \approx 0.17$ (mass fraction). The flame temperature model is based on a classical Burke-Schumann expression:

$$T_{st} = T_1 \frac{Y_{O_2,2}}{r_s Y_{F,1} + Y_{O_2,2}} + T_2 \frac{r_s Y_{F,1}}{r_s Y_{F,1} + Y_{O_2,2}} + (1 - \chi_{R,st}) \frac{\Delta H_F}{c_p} \frac{Y_{F,1} Y_{O_2,2}}{r_s Y_{F,1} + Y_{O_2,2}}$$

(5)

where T_1 and T_2 are the temperatures in the fuel and oxidizer streams feeding the flame, $Y_{F,1}$ and $Y_{O_2,2}$ the mass fractions of fuel and oxygen in those feeding streams, c_p the specific heat of the mixture at constant pressure (assumed constant), ΔH_F the heat of combustion (per unit mass of fuel), and $\chi_{R,st}$ the flame radiant fraction. Equation (5) provides a useful expression of T_{st} as a function of the oxidizer stream properties $Y_{O_2,2}$ and T_2, and may be used to construct a flammability diagram in terms of the vitiated air variables $Y_{O_2,2}$ and T_2 (see [27] for details). Non-flammable (flammable) conditions correspond to sub-critical (super-critical) flame temperatures, *i.e.* flame temperatures such that $T_{st} \leq T_c$ ($T_{st} \geq T_c$). After some manipulations, the following binary expression for the flame extinction factor may be derived [27]:
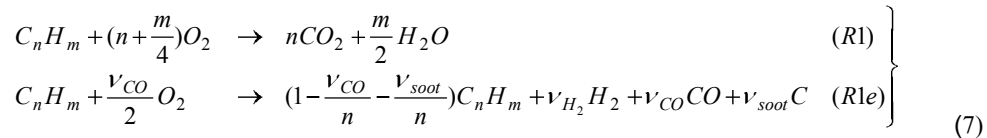
$$FEF = H(\frac{(T_c - T_2)}{(T_c - T_\infty)} - \frac{Y_{O_2,2}}{Y_{O_2,c}})$$

(6)

where H is the Heaviside function, $H(x) = 1$ if $x \geq 0$, $H(x) = 0$ if $x < 0$.

As discussed in [27], Equation (6) is a closure model for *FEF*, provided that the variables $Y_{O_2,2}$ and T_2 are known. The estimation of $Y_{O_2,2}$ and T_2 in Equation (6) is based on a simple search algorithm applied to all computational grid cells in which chemical reaction is taking place. The search algorithm interrogates neighboring cells and the values of $\widetilde{Y}_{O_2}$ and $\widetilde{T}$ in those cells are then used to estimate the vitiated air conditions at the reactive cells location. With this scheme, Equations (4) and (6) provide a combustion model with a flame extinction capability.

3. Modified Combustion and Soot Modeling in FDS5m

We now turn to a presentation of the modifications introduced in FDS5m. The assumption made in Equation (1) that fuel mass does not change in reaction ($R1e$) is inconsistent with the idea that soot leakage across the flame and the subsequent accumulation of black smoke (*i.e.*, cold soot) in the overfire region is likely to be the result of flame extinction phenomena. To account for a partial decomposition of fuel mass into *CO* and soot when extinction occurs, the formulation of reactions ($R1$)-($R1e$) is modified as follows:

$$\left. \begin{array}{rcll} C_n H_m + (n + \frac{m}{4})O_2 & \rightarrow & nCO_2 + \frac{m}{2}H_2O & (R1) \\[2ex] C_n H_m + \frac{\nu_{CO}}{2}O_2 & \rightarrow & (1 - \frac{\nu_{CO}}{n} - \frac{\nu_{soot}}{n})C_n H_m + \nu_{H_2} H_2 + \nu_{CO}CO + \nu_{soot}C & (R1e) \end{array} \right\}$$

(7)

where $\nu_{H_2} = ((m/2) \times (\nu_{CO} + \nu_{soot})/n)$. Reaction ($R1$) corresponds to the ideal transformation of fuel into CO_2 and H_2O, while reaction ($R1e$) corresponds to the partial oxidation/decomposition of virgin fuel into *CO* and soot during extinction of reaction ($R1$). With this modification, the mixture composition is described using three reactive scalars, Z_1, Z_2 and Z_3. These scalars are based on the following decomposition of carbon mass:

$$Z = \underbrace{Y_{C_n H_m}}_{Z_1} + \underbrace{(\frac{W_{C_n H_m}}{n W_{CO_2}})Y_{CO_2}}_{Z_2} + \underbrace{(\frac{W_{C_n H_m}}{n W_{CO}})Y_{CO} + (\frac{W_{C_n H_m}}{n W_{soot}})Y_{soot}}_{Z_3}$$

(8)

where Z_1 and Z_2 represent the carbon mass fraction contained in the fuel and CO_2, while Z_3 represents the carbon mass fraction contained in CO and soot. It can be shown that the entire mixture composition can be reconstructed from the knowledge of Z_1, Z_2 and Z_3 via state relationships. We have in particular: $Y_{soot} = (\nu_{soot} / (\nu_{CO} + \nu_{soot}))(nW_{soot} / W_{C_nH_m})Z_3$. The governing equations for Z_1, Z_2 and Z_3 are simple extensions of Equation (3). The FDS5m closure expressions for $\overline{\dot{\omega}}_{R1}^{m}$ and $\overline{\dot{\omega}}_{R1e}^{m}$ are given by Equation (4); but modifications are introduced in the description of the flame extinction factor FEF in order to account for the effects of fuel type, fuel vitiation and flow time scales. We start by re-writing Equation (5) as:

$$T_{st} = T_1 \frac{Y_{O_2,2}}{r_s Y_{F,1} + Y_{O_2,2}} + T_2 \frac{r_s Y_{F,1}}{r_s Y_{F,1} + Y_{O_2,2}} + (1 - \chi_{R,st}) \frac{Y_{O_2,2} Y_{F,1}(r_s + Y_{O_2,air})}{Y_{O_2,air}(r_s Y_{F,1} + Y_{O_2,2})}(T_{st}^0 - T_\infty)$$

(9)

where $Y_{O_2,air}$ is the oxygen mass fraction in air, and T_{st}^0 the adiabatic flame temperature corresponding to standard (unvitiated) combustion conditions. The expression of T_{st} in Equation (9) depends on air vitiation conditions through $Y_{O_2,2}$ and T_2, fuel vitiation conditions through $Y_{F,1}$ and T_1, and fuel type and flow effects through $\chi_{R,st}$. The air and fuel vitiation conditions are determined by a search algorithm similar to the one discussed in the previous Section. The flame radiant fraction $\chi_{R,st}$ is described as the product of a reference fuel-specific value $\chi_{R,st}^0$ (taken from the literature) times a time scale correction:

$$\chi_{R,st} = \chi_{R,st}^0 \times [0.5 + 0.5 \times \tanh(\frac{(\Delta^2 / \nu_t) - \tau_c}{0.1})]$$

(10)

where τ_c is a critical value of the characteristic flow time scale (Δ^2 / ν_t). The time scale correction is an *ad hoc* expression that is based on recent research on diffusion flame extinction [29]; it assumes that extinction phenomena in pool fires correspond to slow mixing conditions (*i.e.*, long flow time scales) combined with radiation cooling. Consistent with this point of view, we see that in Equation (10), large values of (Δ^2 / ν_t) correspond to large values of the radiant fraction $\chi_{R,st}$, $\chi_{R,st} \to \chi_{R,st}^0$ (and therefore higher probabilities of flame extinction), whereas small values of (Δ^2 / ν_t) correspond to small values of $\chi_{R,st}$, $\chi_{R,st} \to 0$ (*i.e.*, quasi-adiabatic, quasi-complete combustion conditions). The hyperbolic tangent form of the time scale correction and the critical value τ_c are at this point arbitrary; we use $\tau_c = 0.5$ s.

Finally, the expression for the flame extinction factor is: $FEF = H(T_c - T_{st})$, where T_{st} is given by Equations (9)-(10). The modifications presented in equations (7)-(10) provide an enhanced flame extinction capability.

4. Numerical Simulations of Pool Fires

The numerical configuration corresponds to open, wind-free, square-shaped, gaseous fuel pool fires with a prescribed fuel mass loss rate, $\dot{m}_F'' = 0.04 \, \text{kg/m}^2/\text{s}$. The fuel is propylene (C_3H_6); the reference adiabatic flame temperature is $T_{st}^0 = 2334 \, \text{K}$; the reference value of the flame radiant fraction is $\chi_{R,st}^0 = 0.321$ (a choice that corresponds to the value of the global fire radiant fraction χ_R found in small-scale pool fires, see [30]). In the FDS5 simulations, the stoichiometric coefficients for CO and soot are evaluated using prescribed values of the species yields taken from the literature [30]: $\eta_{CO} = 0.017$ and $\eta_{soot} = 0.095$, which gives $\nu_{CO} = \eta_{CO}(W_{C_3H_6} / W_{CO}) = 0.0255$ and $\nu_{soot} = \eta_{soot}(W_{C_3H_6} / W_{soot}) = 0.3325$; the heat of combustion (associated with reaction (R1)) is $\Delta H_F = 41.468 \, \text{MJ/kg}$. The same coefficients ν_{CO} and ν_{soot} are adopted in FDS5m; the heat of combustion is in that case $\Delta H_F^{th} = 44.914 \, \text{MJ/kg}$.

We call H the characteristic dimension of the square burner. A series of numerical simulations was performed for different values of H, $0.4 \leq H \leq 40$ m. The computational grid corresponds to a uniform rectangular mesh. In order to provide maximum grid resolution at reasonable cost, the computational domain is adapted when changing H. For instance, for $H = 0.4$ m, the computational domain is (1 m $\times$ 1 m $\times$ 2.4 m) = (2.5 H $\times$ 2.5 H $\times$ 6 H); the mesh size is (100 $\times$ 100 $\times$ 240), which corresponds to cubic grid cells with a $\Delta = 0.01$ m spacing. In contrast, for $H = 40$ m, the computational domain is (60 m $\times$ 60 m $\times$ 40 m) = (1.5 H $\times$ 1.5 H $\times$ 1 H); the mesh size is (150 $\times$ 150 $\times$ 100), which corresponds to cubic grid cells with a $\Delta = 0.4$ m spacing. Thus, an increased resolution is used in the simulations of the larger pool fires: $(H/\Delta) = 40$

for H = 0.4 m; $(H/\varDelta)$ = 100 for H = 40 m. Simulations are performed on a multi-processor Linux cluster available at the University of Maryland, using the parallel MPI-based version of FDS.

5. Flame Geometry and Computational Grid Requirement

We present in this Section results from the first series of simulations performed with FDS5. The simulations illustrate the fundamental change in flame structure that occurs as H is increased from laboratory- to large-scales. As shown in Figure 1(a), for H = 0.4 m, the combustion zone features a classical cone-shaped single-flame geometry (the flame is the outer edge of the black-colored underfire region); the flame height is several times larger than H, $L_f \approx 3 \times H$; and the flame thickness is approximately $0.5 \times H$. In addition, we note that nonvitiated air is present near almost the entire flame contour (nonvitiated air is colored in white in Figure 1 while vitiated air is colored in grey); this result indicates that the fire is well-ventilated. The pool fire features a similar structure for H = 2 m (Figure 1(b)), except for the fact that the flame is noticeably thinner. More profound changes are observed at larger scales. As shown in Figures 1(c) and 1(d), for H = 10 and 40 m, the combustion zone is broken into several individual flames with a somewhat taller central flame surrounded by smaller flames at the pool periphery; the height of the central flame is of order H whereas that of the flames at the pool periphery is much smaller than H; the individual flames feature an elongated vertical structure and their thickness is also much smaller than H. In addition, we note that the flames are surrounded by vitiated air (the black-colored region is surrounded by thick grey-colored zones); this result confirms that large-scale pool fires are poorly-ventilated.

As discussed in the Introduction Section, this change in flame structure has been previously reported and discussed in the technical literature [16-21]. The increased importance of smaller length scales at larger pool diameters is also consistent with previous measurements of the integral length scale L_t (L_t gives a measure of the size of the energy-containing flow structures; in a Large Eddy Simulation approach, these flow structures must be resolved by the computational grid): for instance, it is found in [31] that in the case of a H = 6 m pool fire, L_t is a small fraction of H, $L_t \approx (H/20)$. This result is consistent with the observations made in Figures 1(c)-(d). When compared to a classical estimate of the integral length scale at small pool diameters, $L_t \approx (H/2)$, this result also suggests that in units made non-dimensional by H, the flow structures in field-scale pool fires are at least an order of magnitude smaller than those found at laboratory-scales.

The implications for computational grid requirements may be described as follows. Assuming a Large Eddy Simulation approach, and using the rule of thumb that adequate grid resolution requires a turbulence-to-grid length scale ratio greater than 10 or 20 (we use 15 hereafter), $(L_t/\Delta) \geq 15$, we find that in small-scale pool fires, where $L_t \approx (H/2)$, the grid requirement may be expressed by the condition: $(H/\Delta) \geq 30$. In contrast, in large-scale pool fires, using the estimate $L_t \approx (H/20)$, we find that the grid requirement becomes: $(H/\Delta) \geq 300$. These estimates indicate that while our sizing of the computational grid may be acceptable for H = 0.4 and 2 m (where we use $(H/\Delta) = 40$ and 50), this choice becomes at best marginal for H = 10 and 40 m (where we use $(H/\Delta) = 100$).

Note that the need for higher grid resolution in simulations of large-scale pool fires has been somewhat overlooked in the literature and that many previous studies correspond in our view to calculations that are significantly under-resolved (see [22-23]). For instance, the study in [22] presents simulations that satisfy the following grid design criterion: $(H/\Delta) \geq (20/(\dot{Q}^*)^{2/5})$; this criterion gives for H = 40 m and $\dot{Q}^* \approx 0.2$: $(H/\Delta) \geq 38$, i.e. a grid requirement that is much weaker than the one discussed above. Thus, while the criterion in [22] correctly predicts the need for finer grids as $\dot{Q}^* \to 0$, it also greatly underestimates the grid resolution requirement.

6. Combustion Efficiency, Soot Yield and Radiant Fraction

We now turn to a discussion of the global fire properties, i.e., the combustion efficiency χ_a, the soot yield η_{soot}, and the radiant fraction χ_R; this discussion starts using results obtained with FDS5 and then
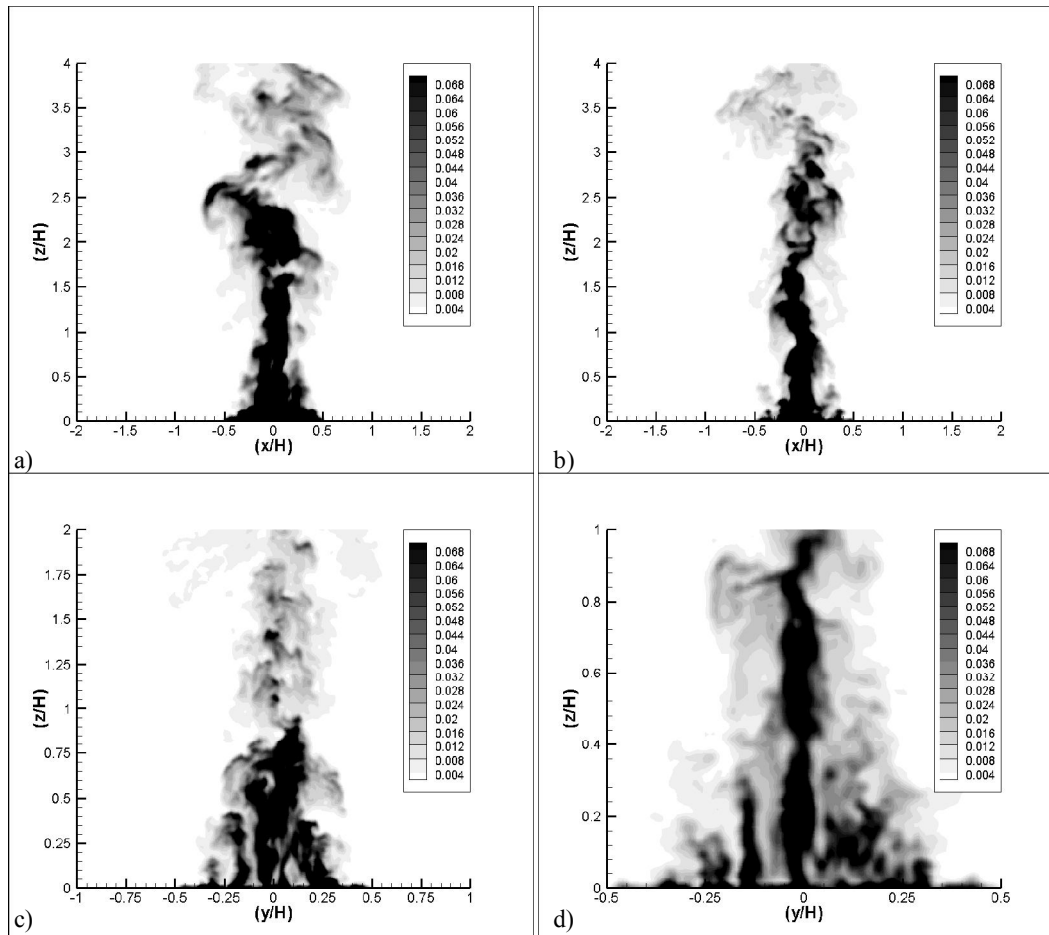
Figure 1. Flame structure in pool fires of increasing size (FDS5 simulations): a) $H = 0.4$ m ($\dot{m}_F \Delta H_F \approx 265$ kW ; $\dot{Q}^* \approx 1.8$); b) $H = 2$ m ($\dot{m}_F \Delta H_F \approx 6.6$ MW ; $\dot{Q}^* \approx 0.8$); c) $H = 10$ m ($\dot{m}_F \Delta H_F \approx 166$ MW ; $\dot{Q}^* \approx 0.35$); d) $H = 40$ m ($\dot{m}_F \Delta H_F \approx 2.65$ GW ; $\dot{Q}^* \approx 0.2$). Instantaneous snapshots showing isocontours of mixture fraction in a central vertical plane. The isolevels are selected so that the region colored in black corresponds to the underfire (i.e., fuel-rich) region and the flame location may be identified as the outer edge of the black region.

continues with results obtained with FDS5m. All global properties are extracted from the FDS simulations by performing spatial- and time-averaging operations: the heat release rate $\dot{Q}$ and overall radiation cooling rate $\dot{Q}_R$ are integrated over the three-dimensional computational domain; the soot mass emission rate $\dot{m}_{soot}$ is integrated over the two-dimensional top boundary of the computational domain (note that in the present Large Eddy Simulation framework, $\dot{m}_{soot}$ is the sum of two components corresponding to convective and diffusive transport); in addition, these quantities are integrated in time over a period of approximately 20 seconds (after steady state has been achieved). As a consistency check, the combustion efficiency is also calculated using two different methods: $\chi_a = \dot{Q}/(\dot{m}_F \Delta H_F^{th})$ and $\chi_a = 1 - (\dot{m}_{Z_1} / \dot{m}_F)$ (FDS5) or $\chi_a = 1 - ((\dot{m}_{Z_1} + \dot{m}_{Z3}) / \dot{m}_F)$ (FDS5m), where $\dot{m}_{Z_1}$ ($\dot{m}_{Z_3}$) designates the mass emission rate of unburnt fuel (CO and soot) tracked by the variable Z_1 (Z_3) (see Equations (2) and (8)); these two methods provide quasi-identical results.

Figure 2 presents the variations of χ_a, η_{soot}, and χ_R with pool size. It is seen that the simulations correctly predict a decrease in radiant fraction with pool size H: χ_R drops from a value of 52% for $H = 0.4$m to a value of 17.5% for $H = 40$ m. Note, however, that according to our discussion in the Introduction Section, these values of □R appear high and while the trends are qualitatively correct, the
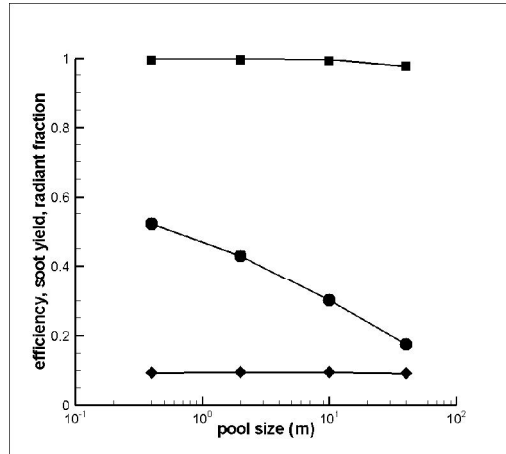
Figure 2. Global properties of pool fires of increasing size H (FDS5 simulations): combustion efficiency χ_a (top curve, squares), radiant fraction χ_R (middle curve, circles), soot yield η_{soot} (bottom curve, diamonds).
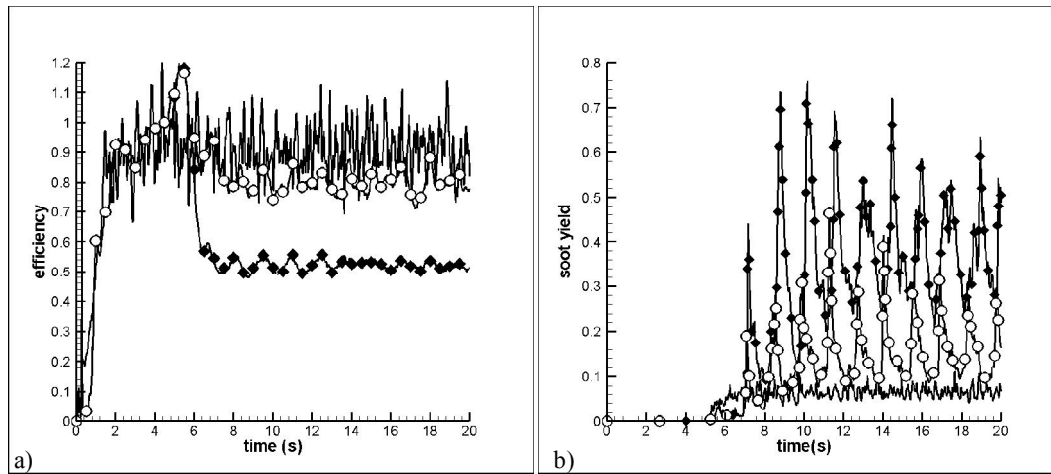

Figure 3. Time evolution of a) the combustion efficiency and b) soot yield in FDS5m simulations. Comparison between simulations corresponding to $H = 0.4$ m (solid line) and 10 m (circles and diamonds).

predictions may not be quantitatively accurate. It is also seen that the simulations do not reproduce the expected decrease in combustion efficiency and increase in soot yield at large values of H; we have in Figure 2: $\chi_a \approx 1$ and $\eta_{soot} \approx 0.094$, independent of H. These results suggest that flame extinction does not play a noticeable role in the overall flame dynamics, a point that was confirmed by further analysis which indicated that while flame extinction is indeed observed in the simulations, and while the FDS5 flame extinction model predicts higher occurrences of extinction at larger-scales because of the more vitiated conditions (Figure 1), these occurrences are consistently followed by re-ignition events that tend to negate their effects.

The absence of H-effects on χ_a and η_{soot} in the FDS5 series of simulations suggest that air vitiation might not be responsible for the experimentally observed changes in combustion efficiencies and soot yields. Alternative candidates to explain variations in χ_a and η_{soot} include fuel vitiation and flow time scale effects. A proposal to incorporate these effects into FDS has been described in the Combustion and Soot Modeling Section above and we now turn to a discussion of the FDS5m results.

Figure 3 presents the time variations of χ_a and η_{soot} in FDS5m simulations corresponding to $H = 0.4$ and 10 m. The $H = 10$ m simulation is performed twice, first using the baseline value of the flame radiant fraction, $\chi_{R,st}^0 = 0.321$, and second using a value that is twice larger. The first 5 seconds in these simulations correspond to an initial phase during which the flame extinction model has been de-activated. At $t = 5$ s, the activation of the flame extinction model leads to a decrease in the combustion efficiency and

to an increase in the soot yield. In contrast to results obtained with FDS5 (Figure 2), the values of χ_a and η_{soot} are now sensitive to H; we get at steady state: $\chi_a \approx 0.91$, $\eta_{soot} \approx 0.065$ for H = 0.4 m (while not shown, these results are not sensitive to the value of $\chi_{R,st}^0 = 0.321$); $\chi_a \approx 0.80$, $\eta_{soot} \approx 0.156$ for H = 10 m and $\chi_{R,st}^0 = 0.321$; and $\chi_a \approx 0.48$, $\eta_{soot} \approx 0.381$ for H = 10 m and $\chi_{R,st}^0 = 0.642$. Note the oscillatory nature of the soot yield signal for H = 10 m (the oscillation frequency is approximately 0.7 Hz).

A careful study identified flow time scale effects (Equation (10)) as the principal modeling ingredient that accounts for the new sensitivity of the predicted χ_a and η_{soot} to changes in H. This result suggests that slow mixing and radiation extinction may be the dominant factors responsible for increased smoke emissions from large-scale pool fires. Note also that the effects of H in Figure 3, while noticeable, remain limited when $\chi_{R,st}^0 = 0.321$. More pronounced effects are obtained by doubling the value of $\chi_{R,st}^0$. Future work will focus on removing some of the *ad hoc* choices made in the flow time scale representation.

7. Conclusions

Numerical simulations of pool fires have been performed for different sizes ranging from laboratory- to field-scales. The numerical simulations are performed using the Fire Dynamics Simulator (FDS) developed by the National Institute of Standards and Technology (NIST). Two series of simulations are performed using both the NIST release of FDS and a modified version in which the flame extinction model has been enhanced to include (along air vitiation effects) fuel type, fuel vitiation, and flow time scale effects.

The simulations reveal the fundamental changes in the fire structure that occur in response to changes in pool size H, *e.g.* the evolution from a single-flame, well-ventilated fire geometry at laboratory scales ($H \leq$ 1-3 m) to a multiple-flame, poorly-ventilated fire geometry at field scales. The increased importance of smaller flames and smaller length scales at larger pool diameters translate into higher computational grid requirements. It is argued that the grid requirement for Large Eddy Simulations of large-scale pool fires may be as high as expressed by the following condition on the pool-size-to-grid-cell length scale ratio: $(H / \Delta) \geq 300$. This requirement is much stronger than previous choices made in the literature.

The simulations also describe the variations of combustion efficiency, soot yield and radiant fraction. It is found that the simulated combustion efficiencies and soot yields are incorrectly insensitive to changes in pool size, unless the flame extinction model includes the effects of flow time scales. This result calls for more elaborate model descriptions of combustion in which the intensity of fuel-air mixing is monitored. This result also provides support to the assumptions made in the proposed extended flame extinction model, in particular the assumptions that: (1) flame extinction in pool fires correspond to slow mixing conditions combined with radiation cooling; (2) flame extinction is the dominant mechanism responsible for soot mass leakage across the flame.

8. References

1. Mudan, K. S., "Thermal Radiation Hazards from Hydrocarbon Pool Fires," *Progress in Energy and Combustion Science*, Vol. 10 (1984), pp. 59-80.
2. Hamins, A., Kashiwagi, T., and Burch, R. R., "Characteristics of Pool Fire Burning," *Proc. Fire Resistance of Industrial Fluids*, American Society for Testing and Materials (ASTM), 1995.
3. Joulain, P., "The Behavior of Pool Fires: State of the Art and New Insights," *Proc. Combustion Institute*, Vol. 27 (1998), pp. 2691-2706.
4. Koseki, H., "Large Scale Pool Fires: Results of Recent Experiments," *Fire Safety Science – Proc. Sixth Intl. Symposium*, International Association for Fire Safety Science, 2000, pp. 115-132.
5. McGrattan, K. B., Baum H., and Hamins, A., "Thermal Radiation from Large Pool Fires," National Institute of Standards and Technology Report NISTIR 6546, Gaithersburg, MD, USA, 2000.
6. Gottuk, D. T., and White, D. A., "Liquid Fuel Fires," SFPE Handbook of Fire Protection Engineering (3rd ed), DiNenno P. J. (ed.), National Fire Protection Association (Quincy, MA, 2002), p. 2/297.
7. Steinhaus, T., Welch, S., Carvel, R. O., and Torero, J. L., "Large-Scale Pool Fires," *Thermal Science*, Vol. 11 (2007), pp. 101-118.
8. Raj, P.K., "LNG Fires: a Review of Experimental Results, Models and Hazard Prediction Challenges," *Journal of Hazardous Materials*, Vol. 140 (2007), pp. 444-464.
9. Koseki, H., and Mulholland, G. W., "The Effect of Diameter on the Burning of Crude Oil Pool Fires," *Fire Technology*, Vol. 27 (1991), pp. 54-65.
10. Notarianni, K. A., Evans, D. D., Walton, W. D., Madrzykowski, D., Lawson, J. R., and Koseki, H., "Smoke Production from Large Oil Pool Fires," *Proc. Sixth Intl. Interflam Conference*, Interscience Communications, 1993, pp. 111-119.

11. Mulholland, G. W., Liggett, W., and Koseki, H., "The Effect of Pool Diameter on the Properties of Smoke Produced by Crude Oil Fires," *Proc. Combustion Institute*, Vol. 26 (1996), pp. 1445-1452.

12. Hamins, A., Konishi, K., Borthwick, P., and Kashiwagi, T., "Global Properties of Gaseous Pool Fires," *Proc. Combustion Institute*, Vol. 26 (1996), pp. 1429-1436.

13. Koseki, H., and Yumoto, T., "Air Entrainment and Thermal Radiation from Heptane Pool Fires," *Fire Technology*, Vol. 24 (1988), pp. 33-47.

14. Koseki, H., Iwata, Y., Natsume, Y., Takahashi, T., and Hirano, T., "Tomakomai Large Scale Crude Oil Fire Experiments," *Fire Technology*, Vol. 36 (2000), pp. 24-38.

15. Yang, J. C., Hamins, A., and Kashiwagi, T., "Estimate of the Effect of Scale on Radiative Heat Loss Fraction and Combustion Efficiency," *Combustion Science Technology*, Vol. 96 (1994), pp. 183-188.

16. Wood, B. D., Blackshear, P. L., and Eckert, E. R. G., "Mass Fire Model: an Experimental Study of the Heat Transfer to Liquid Fuel Burning from a Sand-Filled Pan Burner," *Combustion Science and Technology*, Vol. 4 (1971), pp. 113-129.

17. Zukoski, E. E., "Fluid dynamic aspects of room fires," *Fire Safety Science – Proc. First Intl. Symposium*, Hemisphere Publishing Corporation and Springer-Verlag, 1986, pp. 1-30.

18. Delichatsios, M. A., "Air Entrainment into Buoyant Jet Flames and Pool Fires," *Combustion and Flame*, Vol. 70 (1987), pp. 33-46.

19. Heskestad, G., "A Reduced-Scale Mass Fire Experiment," *Combustion and Flame*, Vol. 83 (1991), pp. 293-301.

20. Zukoski, E. E., "Properties of Fire Plumes," Combustion Fundamentals of Fire, Cox G. (ed.), Academic Press (1995), pp. 101-219.

21. Heskestad, G., "Fire Plumes, Flame Height, and Air Entrainment," SFPE Handbook of Fire Protection Engineering (3rd ed), DiNenno P. J. (ed.), National Fire Protection Association (Quincy, 2002), p. 2/1.

22. Ma, T. G., and Quintiere, J. G., "Numerical Simulation of Axi-Symmetric Fire Plumes: Accuracy and Limitations," *Fire Safety Journal*, Vol. 38 (2003), pp. 467-492.

23. Smith, P., Rawat, R., Spiniti, J., Kumar, S., Borodai, S., and Violi, A., "Large Eddy Simulations of Accidental Fires Using Massively Parallel Computers," *Computational Fluid Dynamics Conf.*, American Institute of Aeronautics and Astronautics, paper no 2003-3697, Orlando, FL, USA, 2003.

24. McGrattan, K. B., Floyd, J. E., Forney, G. P., Baum, H. R., and Hostikka, S., "Improved Radiation and Combustion Routines for a Large Eddy Simulation Fire Model," *Fire Safety Science – Proc. Seventh Intl. Symposium*, International Association for Fire Safety Science, 2003, pp. 827-838.

25. McGrattan, K. B., Hostikka, S., Floyd, J. E., Baum, H. R., and Rehm, R. G., "Fire Dynamics Simulator (Version 5) – Technical Reference Guide," National Institute of Standards and Technology Report NIST Special Publication 1018-5, Gaithersburg, MD, USA, 2007.

26. Magnussen, B. F, and Hjertager, B. H., "On Mathematical Modeling of Turbulent Combustion with Special Emphasis on Soot Formation and Combustion," *Proc.Combustion Institute*, Vol. 16 (1976), pp. 719-729.

27. Hu, Z., Utiskul, Y., Quintiere, J. G., and Trouvé A., "Towards Large Eddy Simulations of Flame Extinction and Carbon Monoxide Emission in Compartment Fires," *Proc. Combustion Institute*, Vol. 31 (2007), pp. 2537-2545.

28. Williamson, J. W., Marshall, A. W., and Trouvé, A. "Developing Extinction Criteria for Fires," *Proc. Eleventh Intl. Interflam Conference*, Interscience Communications, 2007, pp. 849-860.

29. Narayanan, P., and Trouvé A., "Radiation-Driven Flame Weakening Effects in Sooting Turbulent Diffusion Flames," *Proc. Combustion Institute*, Vol. 32 (2007), *in press*.

30. Tewarson, A., "Generation of Heat and Chemical Compounds in Fires," SFPE Handbook of Fire Protection Engineering (3rd ed), DiNenno P. J. (ed.), National Fire Protection Association (Quincy, MA, 2002) p. 3/82.

31. Gritzo, L. A., Sivathanu, Y. R., and Gill, W., "Transient Measurements of Radiative Properties, Soot Volume Fraction and Soot Temperature in a Large Pool Fire," *Combustion Science and Technology*, Vol. 139 (1998), pp. 113-136.

Author Biography

Dr. Arnaud Trouvé is Associate Professor in the Department of Fire Protection Engineering at the University of Maryland, College Park, U.S.A. Arnaud's primary research focus and experience is in the field of multi-dimensional numerical modeling for turbulent combustion applications; Arnaud is active in different application areas of Computational Fluid Dynamics, including High-Performance Scientific Computing, direct numerical simulation and large eddy simulation, and different application areas of combustion, including fire and explosion safety, IC engines and gas-turbine engines. Arnaud is actively involved in the international combustion science and fire science communities; he is Associate Editor of Combustion, Theory and Modelling and of the Proceedings of the International Symposium on Combustion.